6th AIAA Flow Control Conference
25 - 28 June 2012, New Orleans, Louisiana

AIAA 2012-2947

Separation Control Using Dielectric Barrier Discharge-Induced Suction and Vortex Generation

[*]Seong-kyun Im[1], [*]Moon Soo Bak[2], [*§]M. Godfrey Mungal[3] and [*]Mark A. Cappelli[4]
[*]*Mechanical Engineering Department, Stanford University, Stanford, California, 94305*
[§]*School of Engineering, Santa Clara University, Santa Clara, California, 95053*

We investigate the characteristics of vortices induced by spanwise forcing using a streamwise oriented dielectric barrier discharge (DBD) with and without a boundary layer suction channel, the flow of which is also driven by a DBD. The velocity field over various regions in the vicinity of the actuator is obtained by ensemble averaging particle image velocimetry. Increased boundary layer thinning and a stronger downward motion are seen near the powered flow-exposed electrode when the DBD is used in conjunction with a suction slot. The effect of varying the applied voltage and freestream velocity on the induced flow is examined. Studies are carried out on the ability for such a structure to control separation on an inclined flat plate and ramp. We find that DBD actuation together with boundary layer suction leads to more robust separation control in these adverse pressure gradient configurations.

I. Introduction

The use of boundary layer suction as a method of controlling boundary layer characteristics has been studied for more than a century.[1] Boundary layer suction leads to aerodynamic flow control through its influence on boundary layer displacement and momentum thickness and the ability to suppress flow separation[2,3], re-laminarization of boundary layer turbulence[4], and lift enhancement and drag reduction[5,6]. Boundary layer control using boundary layer suction is still an active field of research despite its long history. The principle of boundary layer suction is that the low speed fluid in the inner boundary layer is removed through slots or porous material[7] in regions of adverse pressure gradients. Usual methods of employing boundary layer suction require a pumping device which adds weight and complexity to the aircraft. A boundary layer suction mechanism that does not employ moving parts is highly desired. In this paper, we demonstrate the development of such a device, which makes use of dielectric barrier discharge (DBD) plasma actuators.

DBD actuators for aerodynamic control applications have been studied extensively ever since their first introduction by Roth et. al.[8] A single DBD actuator consists of exposed and dielectric-covered electrodes driven by alternating current (AC), oriented to induce a directional flow of neutral gas through collisions with the drifting ions. There have been experimental reports that describe this directional flow as having a "suction" - like effect on the flow[9], resulting in boundary layer re-attachment[10-12], boundary layer transition delay[13], boundary layer thinning in subsonic[14] and supersonic flow[15], and flow separation control[16]. We note however, that DBD actuators, in their usual configuration, displace low speed fluid with higher speed fluid from the freestream region, however, they do not remove this displaced fluid entirely from the boundary layer region. In this study, we describe the introduction of a suction channel, also with internal DBD actuation, that removes this low speed fluid altogether, enhancing flow control authority.

[1] Graduate Student, AIAA Student Member.
[2] Graduate Student.
[3] Professor. AIAA Associate Fellow.
[4] Professor.

II. Experimental Setup

The experiment, depicted in Fig. 1, consists of a DBD actuator fabricated into flat plate and a PIV system to measure velocity fields. A 20 degree wedged flat plate (130 mm wide 230 mm long) is located in the center of a w = 300 x H = 300 mm cross sectional area vertical wind tunnel that can generate up to 5.5 m/s base flow (Re_w = 104000). A symmetric DBD actuator pair is integrated into the top surface of a flat acrylic plate as illustrated in the top view of Fig. 2 (a) and cross sectional view of Fig. 2 (b). The acrylic plate (5 mm thick) uses Kapton tape (50 µm thick) as a dielectric layer to isolate the embedded electrode. The exposed electrode is a single copper strip oriented parallel to the base flow. These electrodes (exposed and embedded, each 0.1 mm thick) are 135 mm in length and 7 mm wide, and 135 mm in length and 50 mm wide, respectively. The direction parallel to the flow is noted as the y-direction and spanwise to the flow is the x-direction. The direction perpendicular to the flat plate is the z-direction. The origin of this coordinate system is set to be at the center of the leading edge (i.e. (x,y,z) = (0,0,0) at the center of leading edge of the flat plate). The exposed electrode is centered over the buried electrode, and both electrodes are placed along the center of the model 50 mm downstream (y = 50 mm, x = 0 mm) from the leading edge. Sand paper (120 Grit, 130 mm wide and 20 mm long) is attached to the top of the flat plate at a distance y = 5 mm downstream from the leading edge to serve as a boundary layer trip, creating a turbulent boundary layer flow. Two parallel suction slots (1.5 mm wide) straddle the exposed electrode, 1 mm from either side (i.e. 5 mm from center of flat plate: x = ± 5 mm). These slots lead to a 2 mm high inner channel which carries away the drawn fluid eventually bleeding this fluid into the freestream at the side of the model, as schematically shown in Fig. 2 (b). Two additional asymmetric DBD actuator pairs are built into the inner (upper) surface of this channel to drive this internal flow. The exposed electrodes in each of these additional actuator pairs are located at x = ± 35 mm while the embedded electrodes, encapsulated with Kapton tape are placed at x = ± 42 mm from the center of flat plate. Both exposed and embedded electrodes are 7 mm wide and 115 mm in length. Cast acrylic (1.5 mm thick) and Kapton tape (50 µm thick) are used as the dielectric barrier for these internal asymmetric actuators. In this configuration, the main electrode pair serves to produce a symmetric spanwise forcing, producing a downward suction (see Fig. 2 (b)) leading to a displacement of the boundary layer flow by the higher speed fluid. A portion of the slower boundary layer fluid is then swallowed by the adjacent slots and pushed laterally within the internal channel by the asymmetric actuators creating a forced internal flow, much in the same way that a pump drives a suction flow in a more conventional system. This structure is used to study its ability to control flow separation. Two cases of separation were investigated, as shown schematically in Fig. 3. The first (Fig. 3a)) is separation on the same plate but inclined at an angle of 8 degrees relative the free stream flow. The second (Fig. 3b)) is separation on a 25 degree ramp downstream of the DBD embedded flat plate oriented parallel to the flow. This ramp has the same width as the flat plate and is 200 mm long. Details of these separation control studies are presented later in the paper.

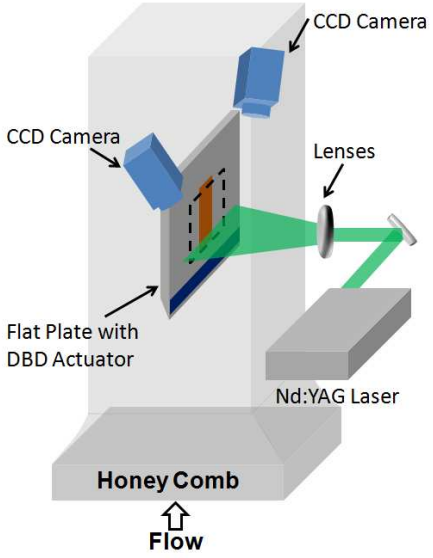

Figure 1. Schematic of experimental setup

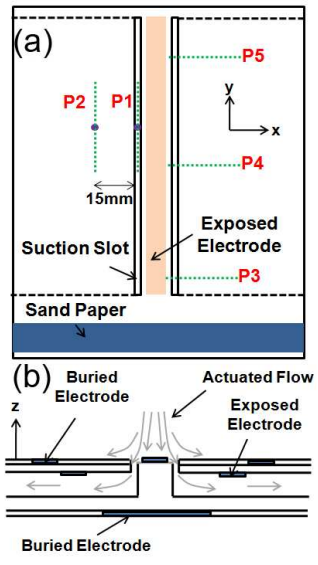

Figure 2. Schematic of DBD suction actuator model.

Two independent AC power supplies are used to power the dielectric barrier discharges. The main external flow symmetric actuator is driven by a Minipuls 6 power supply. In this study, the operating voltage and frequency are 12

- 16.5 kV (peak-to peak) and 15 kHz, respectively. The power consumption of the primary electrode pair is about 13 - 18W, depending on the driving voltage. The two asymmetric actuators inside the suction slot bleed channels are powered by an Information Unlimited PVM 300 generator with a fixed driving voltage and frequency of 12 kV (peak-to peak) and 25 kHz, respectively. The power consumed by these internal electrode pairs is ~ 15W.

A Nd:YAG laser (New wave, Gemini PIV, 100mJ/pulse energy, 10Hz, 532 nm) is shaped into a thin sheet (~ 300 μm) using two cylindrical lenses and a convex spherical lens, and is directed into the test section for the PIV studies. The scattering is recorded from two 2D imaging planes (P1 and P2, x = -5, -15 mm) and from three planes (P3 to P5, y = 60 mm, 110 mm, and 160 mm) which are perpendicular to P1 and P2 as depicted in Fig. 2 (a) and Fig. 2(b). The region captured in the P1 and P2 images span a distance y = 125 mm to y = 145 mm and is z = 10 mm in height. The region captured in the P3 to P5 images span a distance x = 3 mm to x = 33 mm and is z = 30 mm in height. Two (P6 and P7) and three (P8 to P10) more planes are used to record PIV images for the separation on the inclined flat plate and on the 25 degree flap downstream of the DBD actuator, as shown in Fig. 3 (a) and (b) respectively. The regions captured in the imaging plane for P6 and P7 are at the center plane of the flat plate (x = 0 mm) and span a 45 mm (in y-direction) by 30 mm (in z-direction) region of interest starting at y = 50 mm and 90 mm, respectively. P8 to P10 planes begin at y = 230 mm and span a 40 mm (in y-direction) by 30 mm (in z-direction) region of interest. P8 to P10 planes are located at x = 0 mm, -5 mm, and -25 mm, respectively.

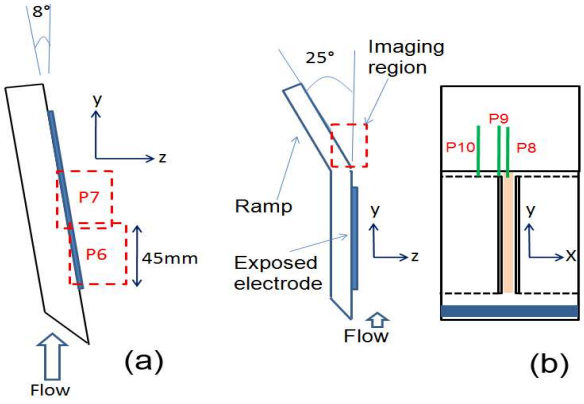

Figure 3. (a) Schematic of inclined flat plat model, (b) Schematic of angled ramp model.

In addition to quantifying the velocity field, the results from P1 and P2 are used to investigate the boundary layer at the location y = 135 mm from leading edge. Without flow actuation, the boundary layer thickness in this region is about 9 mm, giving rise to a local Reynolds number (based on this boundary layer), Re_δ = 2180. For the PIV diagnostics, double exposure CCD cameras (La Vision, Imager Intense) capture the scattered light from aluminum oxide particles. The velocity vector field is obtained from two instantaneous sequential images taken with a 50 μs time delay. Laser shot timing and the triggering of the camera are synchronized by DaVis 7 software. PIV images are taken with three different flow conditions: (Case 1) flow without actuation, (Case 2) flow with actuation (i.e. suction induced by the DBD actuators within the bleed channel), and (Case 3) flow with actuation but with the suction slots blocked. The two asymmetric channel actuators are not activated in Case 3.

III. Results

A. Characteristics of induced flow

The mean vertical velocity profile at y = 135 mm for Case 1 to 3 at the P1 and P2 imaging regions obtained by ensemble averaging 100 instantaneous PIV images are shown in Fig. 4 for a freestream velocity of 3.8 m/s (Re_w = 72,000). It is apparent from the mean velocity profile for the P1 plane in Fig. 4 that DBD actuation draws higher momentum fluid from the freestream into the boundary layer in the vicinity of the exposed electrode by comparing Case 1 (blue circles) to Case 2 (red crosses). The boundary layer is thinned from δ_{Case1} ~ 9 mm to δ_{Case2} ~ 2 mm and the momentum thickness is reduced from θ_{Case1} ~ 1.09 mm to θ_{Case2} ~ 0.32 mm. Boundary layer thinning is more dramatic in Case 2 (red crosses) compared to Case 3 (green squares), i.e., the case when the central symmetric DBD is actuated, but the bleed channels are blocked and internal actuators are inactive. In the absence of the internal channel DBD-driven boundary layer bleed, the flow-exposed DBD reduces the momentum thickness to θ_{Case3} ~ 0.83 mm but only thins the boundary layer thickness by about 1 mm less than that without actuation. A similar but correspondingly weaker flow response is observed in the P2 plane located x = -15 mm. Again, the DBD actuation

draws higher momentum flow to the vicinity of the wall as seen when comparing Case 1 (blue circles) to Case 2 (violet diamonds). However, the effect of this actuation is not as strong as that seen in the plane closer to the slot. The result for Case 3 (light blue reverse triangles) indicates that the actuation resulting from just the flow-exposed DBD results in lost benefit at this plane.

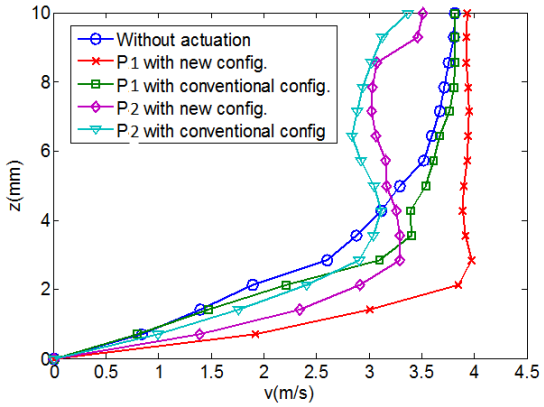

Figure 4. Mean velocity profile for the P1 and P2 imaging planes 135mm from the leading edge.

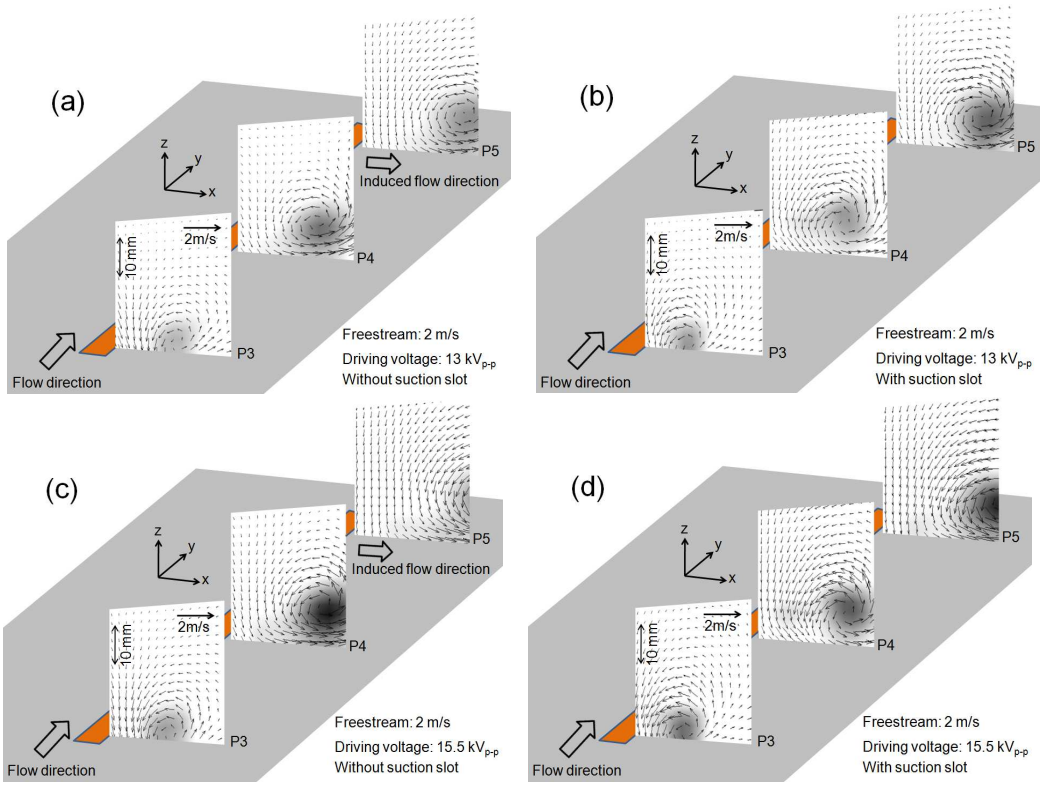

Figure 5. Mean velocity field at 2 m/s freestream speed with 13 kV_{p-p} driving voltage (a) without suction, and (b) with suction, (c) 15.5 kV_{p-p} driving voltage without suction, and (d) with suction.

Velocity fields for Case 2 and 3 (flow exposed DBD but with/without active boundary layer bleed) of regions P3 to P5 are obtained by ensemble averaging 250 stereo PIV image pairs. These are shown in Fig. 5. The direction of the freestream flow and coordinates in these images are shown with arrows. The two flow components (x, z - direction) are depicted by arrows whereas vorticity is represented by black and white contours. PIV results in the P3 to P5 imaging planes for Case 2 and 3 flow conditions (with 13 kV_{p-p} applied voltage, at 2 m/s freestream flow) are depicted in Fig. 5 (a) and (b), respectively. Vortex formation is observed, as expected, in Fig. 5 (a). The spanwise

forcing produced by the DBD actuator is clearly evident. The resulting motion induces a local circulation which grows in strength and size along the flow direction. As this circulation grows, the vortex convects away from the exposed electrode and lifts away from the wall. This observation is consistent with the study by Juke et al.[16] In the presence of the suction slot, however, the process of vortex formation and propagation appears to have different characteristics, as seen in Fig. 5 (b). There is a stronger downward and counter clockwise motion near the electrode. As a result of this motion, the vortex forms closer to the electrode and the wall than without the active suction slot. Since the actuation from the DBD is not perpendicular to the suction slot and an image vortex exists in the wall, there is x-directional forcing that makes the vortex migrate away from the electrode (x-direction), as described schematically in Fig. 2 (b). Results with slightly higher driving voltage (~15.5 kV_{p-p}) for the free-stream exposed pair and the same freestream speed are depicted in Fig. 5 (c) and (d) for Case 2 and 3, respectively. They appear to be qualitatively similar to those of the lower voltage. However, there is stronger fluid motion due to the increased force and the induced vortices migrate and lift further away in the x and z direction, respectively. The size and strength of the vortex is larger than that of lower driving voltage case.

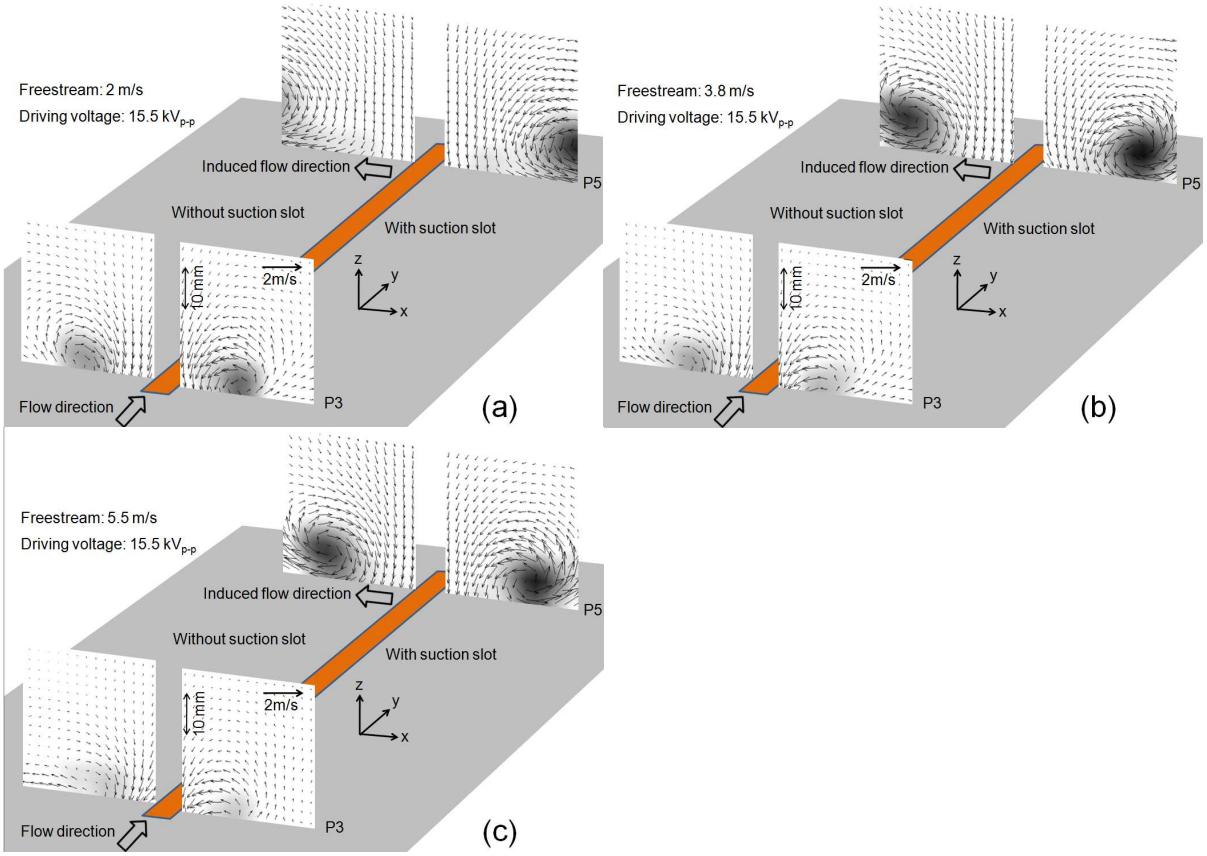

Figure 6. Mean velocity field at P3 and P5 imaging planes with 13 kV_{p-p} driving voltage without and with suction case for (a) 2 m/s, (b) 3.8 m/s, and (c) 5.5 m/s freestream speed.

The effect of freestream speed on the induced flow is presented in Fig. 6 (a) - (c). Here, freestream speeds are varied between 2 m/s, 3.8 m/s, and 5.5 m/s, while keeping the external flow DBD driving voltage at 15.5kV_{p-p}. Velocity fields for the P3 and P5 imaging planes for Case 2 (with an active suction slot) and Case 3 (inactive suction) flow conditions are acquired by ensemble averaging 250 stereo PIV image pairs and are depicted in the right and left hand side of main exposed electrode, respectively to facilitate comparisons. The general process of vortex formation remains the same as that seen in Fig. 5 but the characteristics of the vortices are different for each freestream speed case studied. As the speed increases, the downward motion in the P3 plane for Case 2 and 3 flow conditions decreases. As seen in Fig. 6, the Case 2 flow condition (right side of figures) gives rise to induced vorticity that remains closer to the wall and to the electrode when compared to Case 3 (left side of figures), and the strength of the vortices for all speeds appear stronger than that with the blocked and inactive suction channel. We see that with increasing speed, the lateral (x) displacement of the vortices is reduced for any axial (y) position. This is attributed to a reduced residence time of the flow to actuation. We also note however, that the actuation power

itself is affected by the change in flow speed. Visual observations of the discharge itself indicate that the active length of the discharge and its emission intensity diminishes as the freestream speed increases. This is expected to result in reduction in actuator effectiveness as previously reported by Borghi et al.[17]

B. Separation control

The combined downward directed and suction bleed flow induced by DBD actuation is examined for its ability to control separation under two flow configurations. The first, is that of the flat plate described above with embedded actuators and bleed channel, but tilted by 8° relative to the free stream. The 2D velocity fields, obtained by ensemble averaging 250 instantaneous PIV image pairs, for imaging planes P6 and P7 described in Fig. 3 (a) with Case 1 and 2 conditions at 3.8 m/s freestream flow are depicted in Fig. 7 (a). The streamlines for each case are shown in Fig. 7 (b). Flow conditions and imaging planes are marked in the figure accordingly. Arrows in this figure represent the velocity components in the y-z plane whereas the color map is just the y-component velocity. There is a region of recirculation in the P6 imaging plane for the Case 1 flow condition confirming the presence of a separation bubble. The flow reattaches by the center of the P7 imaging plane. With the DBD actuation (Case 2), see Fig. 7 (a), the flow reattaches further upstream than in the Case 1 flow condition. This is also evident from the resulting streamlines as seen in Fig. 7 (b). The downward motion induced by the freestream exposed actuator is apparent in the Case 2 flow condition at both the P6 and P7 planes. Considering that this suction that is induced by the DBD actuators begins near the upstream boundary of the P6 imaging plane, it appears then that there is an immediate influence of this suction on separation.

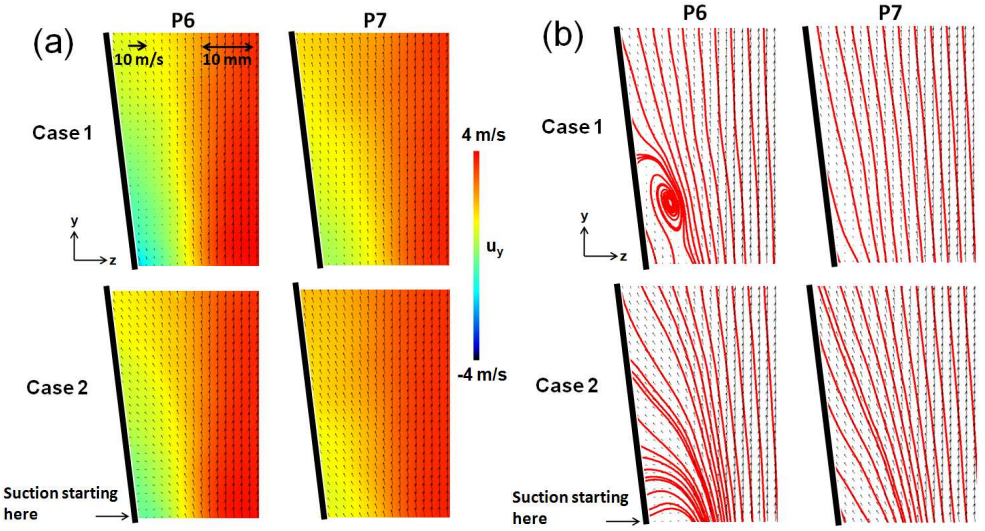

Figure 7. (a) Mean velocity profile, and (b) Streamline for P6 and P7 imaging planes with Case 1 and 2 flow conditions at 3.8 m/s freestream speed.

The second configuration for which separation control is examined with the 25° ramp, positioned just downstream of the flat plate, as shown in Fig. 3 (b). Figure 8 (a) - (c) depict the velocity fields obtained by averaging 250 PIV image pairs for the P8 imaging plane with 15.5 kV_{p-p} driving voltage at 2 m/s, 3.8 m/s, and 5.5 m/s, respectively. Each of the three flow conditions (Cases 1 -3) are studied. The color map in these figures depict the velocity magnitude (normalized by the freestream speed). The presence of a separated region is clearly visible without actuation (Case 1). The separated flow is weakened with DBD actuation and suction (Case 2). It is interesting to note that the effect is enhanced (in this plane) as the freestream speed is increased. We believe that this is due to the fact that the vortex generated by the DBD places it closer to the region examined by the P8 plane as the freestream speed increases. The effect of actuation diminishes when the suction slots are blocked (Case 3) indicating that the bleeding of the boundary layer plays a major effect on control of the separation.

The streamwise mean velocity field for the P8 to P10 imaging planes acquired by averaging 250 PIV image pairs with 15.5 kV_{p-p} driving voltage and 5.5 m/s freestream flow speed are shown in Fig. 9 (a) - (c), respectively. The color map in these figures depict the velocity magnitude (normalized by freestream speed). The velocity field without actuation is only shown once (top left) because the streamwise mean velocity field for the three different planes are essentially indistinguishable. The influence on the flow by DBD actuation is observed in all planes when there is an active suction slot (Case 2). However, the effectiveness is not nearly as strong in the case when the slot is blocked (Case 3). The Case 3 effectiveness improves for planes P9 and P10 because of the arrival of the vortex generated by the flow exposed DBD to these PIV planes, but the strength of the vortex is less than that when the

suction slots are active, as seen in the detailed studies of the vortex generation and displacement as depicted earlier in Figs. 5 and 6.

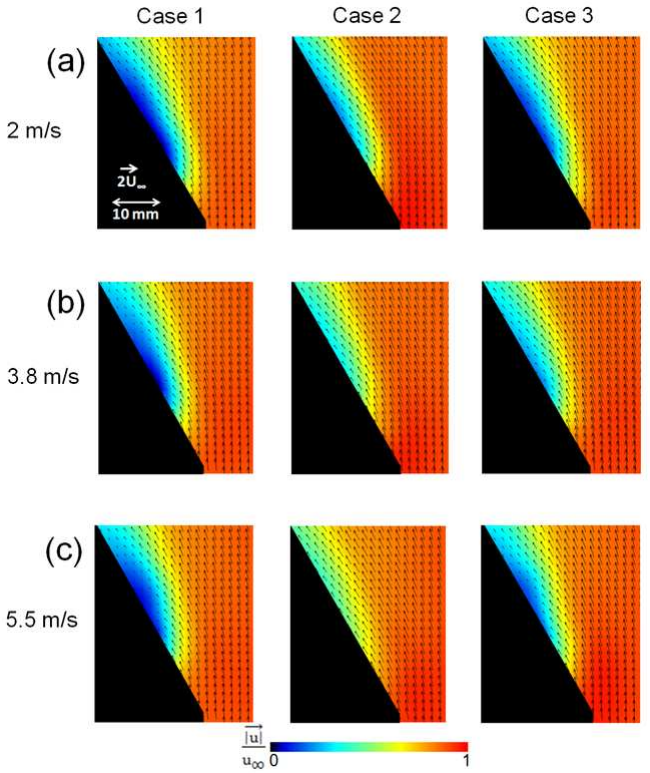

Figure 8. Mean velocity profile for the P8 imaging plane with Case 1, 2 and 3 flow conditions at (a) 2 m/s, (b) 3.8 m/s, and (c) 5.5 m/s freestream speed.

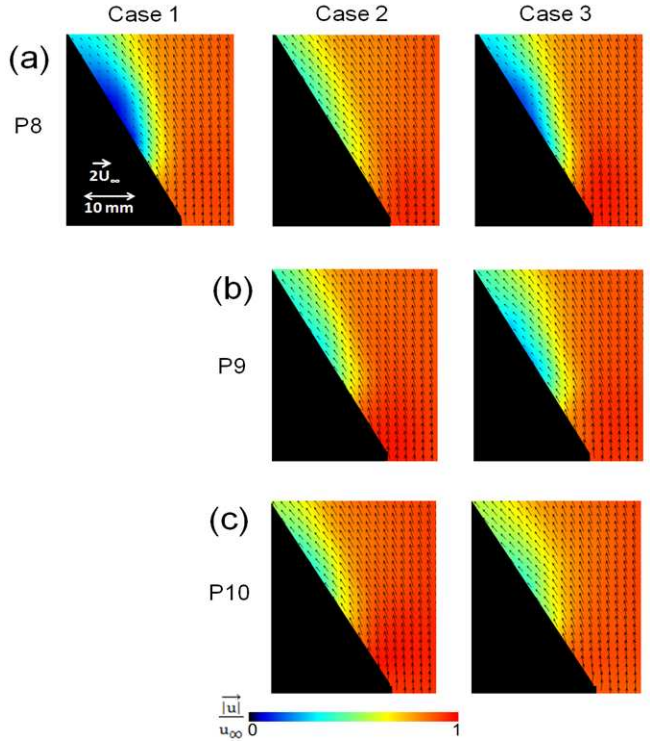

Figure 9. Mean velocity profile for (a) P8, (b) P9, and (c) P10 imaging planes with Case 1, 2 and 3 flow conditions at 5.5 m/s freestream speed.

IV. Conclusion

We have carried out experiments that characterize flow induced by a streamwise-aligned dielectric barrier discharge designed to impart symmetric spanwise forcing and to generate streamwise vorticity. Suction slots also driven by dielectric barrier discharges are used in conjunction with the DBD vortex generators to enhance boundary layer actuation. Vortices induced by the DBD actuation with the suction slots activated generate strong surface-directed motion in the vicinity of the external flow DBD electrode. Higher discharge voltage results in stronger induced flow and increased vorticity. An increase in freestream speed is found to result in lower vorticity and a weaker downward surface-directed motion and the trajectory of the vortex is much closer to the wall and exposed electrode. The reduction in the flow residence time in the discharge-active region is speculated to play a role in the recorded flow behavior.

The spanwise DBD actuation with active suction was tested for its ability to re-attached separated flows on a flat plate inclined at 8^o to an incoming flow and on an aligned flat plate with a 25^o trailing ramp. In both cases, the activated suction slot increased the ability to re-attach the separated boundary layer flows over a range of free stream velocities.

Acknowledgments

This research is supported by the Stanford Predictive Science Academic Alliance Program (PSAAP) Center, funded by the Department of Energy (National Nuclear Security Administration) under Award Number DE-FC52-08NA28614.

References

[1]Schlichting H., "Boundary Layer Theory," New York, Mcgraw-Hill, 1955.

[2]Sano M., Hirayama N., "Turbulent Boundary Layers with Injection and Suction through a Slit," *Bull. JSME*, Vol. 28, 1976, pp. 807-814.

[3]Gbadebo S. A., Cumpsty B. A., and Hynes T. P., "Control of Three-dimensional Control Using Surface Dielectric Barrier Discharges," *Journal of Turbomachinery*, Vol. 130, 2008, pp. 011004.

[4]Antonia R. A., Zhu Y., and Sokolov M., "Effect of Concentrated Wall Suction on a Turbulent Boundary Layer," *Physics of Fluids,* Vol. 7, 1995, pp. 2465-2474.

[5]Park J., and Choi H., "Effects of Uniform Blowing or Suction from a Spanwise Slot on a Turbulent Boundary Layer Flow," *Physics of Fluids*, Vol. 11, 1999, pp. 3095-3105.

[6]Badrinarayanan M. A., "An Experimental Study of Reverse Transition in Two-dimensional Channel Flow," *Journal of Fluid Mechanics*, Vol. 31, 1968, pp. 609-623.

[7]Moffat R. J., and Kays W. M., "The Turbulent Boundary Layer on a Porous Plate: Experimental Heat Transfer with Uniform Blowing and Suction," *International Journal of Heat and Mass Transfer*, 1968, Vol. 11, pp. 1547-1566.

[8]Roth J. R., Sherman D. M., and Wilkinson S. P., "Boundary Layer Flow Control with a One Atmosphere Uniform Glow Discharge Surface Plasma," *36th AIAA Sciences Meeting and Exhibit*, 1998, AIAA 1998-0328.

[9]Moreau E., "Airflow Control by Non-thermal Plasma Actuators," *Journal of Physics D: Applied Physics*, Vol. 40, 2007, pp. 605-636.

[10]Post M. L., and Corke T. C., "Separation Control on High Angle of Attack Airfoil Using Plasma Actuators," *AIAA Journal*, Vol. 42, 2004, pp. 2177-2184.

[11]Sung Y., Kim W., Mungal M. G., and Cappelli M. A., "Aerodynamic Modification of Flow Over Bluff Objects by Plasma Actuation," *Experiments in Fluids*, Vol. 42, 2006. pp. 479-486.

[12]Do, H., Kim, W., Mungal, M. G., and Cappelli, M.A., "Bluff Body Flow Separation Control using Surface Dielectric Barrier Discharges," *45th AIAA Aerospace Sciences Meeting and Exhibit*, 2007, AIAA 2007-939.

[13]Grundmann, S., and Tropea, C., "Experimental Transition Delay Using Glow-Discharge Plasma Actuators," *Experiments in Fluids*, Vol. 42, 2007, pp. 653-657.

[14]Porter, C. O., Baughn, J. W., McLaughlin, T. E., Enloe, C. L., and Font, G. I., "Plasma Actuator Force Measurements," *AIAA Journal*. Vol. 45, 2007, pp. 1562-1570.

[15]Im, S., Do, H., and Cappelli, M. A., "Dielectric Barrier Discharge Control of a Turbulent Boundary Layer in a Supersonic Flow," *Applied Physics Letters*, Vol. 97, 2010, pp. 041503.

[16]Jukes T. N., and Choi K-S., "Dielectric-Barrier-Discharge Vortex Generators: Characterisation and Optimisation for Flow Separation Control," *Experiments in Fluids*, Vol. 52, 2012, pp. 329-345.

[17]Borghi C. A., Carraro M. R., Cristofolini A., and Neretti G., "Electrohydrodynamic Interaction Induced by a Dielectric Barrier Discharge," *Journal of Applied Physics*, Vol. 103, 2008, pp. 063304.